Characteristics of muonic and electromagnetic components far from the core of giant air showers above 10^{18} eV

K. Honda,[1] K. Hashimoto,[1] N. Kawasumi,[1] T. Kutter,[2] M. Nagano,[3] and I. Tsushima[1]
[1]*Faculty of Education, Yamanashi University, Kofu 400, Japan*
[2]*Department of Physics, University of Heidelberg, Heidelberg, Germany*
[3]*Institute for Cosmic Ray Research, University of Tokyo, Tokyo 188, Japan*
(Received 4 December 1996)

In order to know the relative proportion of electrons, photons, and muons far from the cores of giant air showers, a detector with two scintillators sandwiching a lead plate of 1 cm thickness (leadburger) has been built and placed at one corner of the Akeno Giant Air Shower Array (AGASA). Results obtained from data collected over an 18-month run are reported here. Lateral distributions and arrival time distributions of electrons, photons, and muons at around 1000 m–2500 m from the core for showers of energies larger than $10^{18.0}$ eV have been determined. Our observations show that muons may be separated from electromagnetic components far from the shower core with a lead layer of 1 cm thickness, as suggested from Monte Carlo simulations using the MOCCA program. These studies show the MOCCA program to be a powerful simulation tool for further development of the detector design for the Pierre Auger project. [S0556-2821(97)03219-0]

PACS number(s): 96.40.De, 96.40.Pq

I. INTRODUCTION

It has been suggested that there might be a cutoff in the energy spectrum of primary cosmic rays around 10^{20} eV, if they are of extragalactic origin, since cosmic rays would lose energy during their travel in intergalactic space as a result of their interaction with the universal background radiation. This cutoff is called the GZK cutoff after predictions by Greisen [1] and Zatsepin and Kuźmin [2].

To detect this cutoff in the primary energy spectrum, several experiments have been performed during the last 30 years and the significance of the evidence for the GZK cutoff has increased. That is, only a small number of cosmic rays exceeding 10^{20} eV have been observed, compared with an expectation of more than 25 if there were no cutoff and the spectrum were to extend beyond 10^{20} eV with the same slope [3]. The extragalactic origin of the highest energy cosmic rays is also supported by the observed uniform distribution over the celestial sphere and the flattening of the primary energy spectrum around 10^{19} eV.

However, recent observations of a 3×10^{20} eV cosmic ray by the Fly's Eye detector [4] and of a 2×10^{20} eV one by the Akeno Giant Air Shower Array (AGASA) [5], well beyond the expected cutoff energy, have posed a puzzle concerning their origin. Furthermore, a fraction of the observed cosmic rays above 4×10^{19} eV appear to be a part of few clusters with arrival directions within a limited space angle, which suggests the presence of rather weak intergalactic magnetic fields between the sources and Earth, if these particles are assumed to be protons [6]. These observations point to the necessity of performing the next generation of experiments for resolving these puzzles.

Since the flux of cosmic rays in the highest energy region is very small, the construction of two large arrays, covering 3000 km^2 area each, one in the Northern and the other in the Southern hemisphere, has been proposed [7]. Each array is expected to observe more than several 10^3 showers of energies greater than 10^{19} eV per year. According to the results of shower simulations by Cronin [8] using the MOCCA program developed by Hillas [9], the electromagnetic components, namely, the photons and electrons, are very soft at large distances from the core ($r>1000$ m), while the muonic component has a mean energy of around 1 GeV. Figure 1 shows these results for energy distributions of photons, electrons, and muons at 1410 m from the core for proton, iron, and γ-ray primaries of 10^{19} eV.

Since the muons arrive at the earliest time while the soft electromagnetic components are spread over a few μsec (Fig. 2 [8]), the arrival time measurement for each particle may also be helpful in separating the muon from the electromagnetic component.

In order to separate muons from electromagnetic components, a water tank of 10 m^2 area and 1.2 m depth has been selected as a prototype detector for the Auger Project [10]. However, during the Auger Design Workshop, a detector using two layers of thin scintillators, between which a lead layer of thickness of a few radiation lengths has been inserted, has also been investigated as a possible candidate for the Auger array [10]. Such a detector with a Sc-Pb-Sc sandwich configuration is referred to hereafter as a ''leadburger.''

Before assessing the usefulness of a prototype detector for the study of the highest energy cosmic rays, it is essential to examine the validity of the results obtained from simulations in reproducing the observed features of extensive air showers at great distances from the core for such low energy particles. The purpose of the present experiment, therefore, is to study the electromagnetic and muon components of very low energy at far distances from the core of giant air showers of energies above 10^{18} eV.

II. EXPERIMENT

The prototype of a leadburger has been built at the southeast corner of the (AGASA) [11] by using available detectors at Akeno. The AGASA consists of 111 scintillation detectors

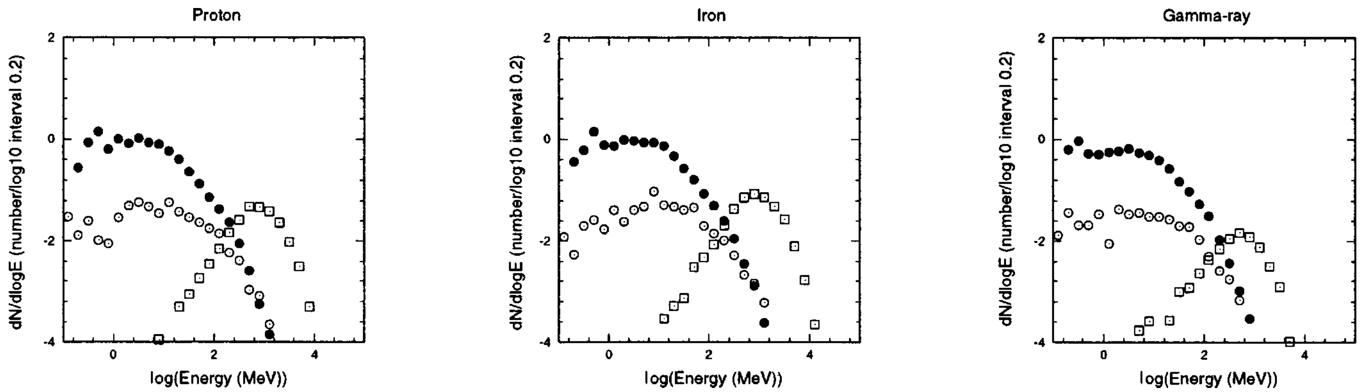

FIG. 1. Energy spectra for muons (open squares), photons (solid circles), and electrons (open circles) in a shower of 10^{19} eV, initiated by a proton, an iron nucleus, or a γ-ray primary, at a core distance of 1410 m [8].

of 2.2 m^2 area deployed over 100 km^2 area. At the same corner, there is another array called the ''1 km^2 array'' which consists of 156 scintillation counters of 1 m^2 area each and 8 muon detectors, each of 25 m^2 area. The leadburger is installed at the center of the 1 km^2 array. The 1 km^2 array along with the leadburger is triggered by the AGASA.

The detector, covering an area of 12 m^2, is segmented into 2×12 plastic scintillation counters (up to April 6, 1995, 10 m^2), each with an area of 1 m^2 as shown in Fig. 3. The lead layer has a thickness of 1 cm corresponding to about 1.8 radiation lengths.

Each scintillation counter is equipped with a 5 inch photomultiplier (Hamamatsu R1512 or R1608), a preamplifier, and a main amplifier. The seventh dynode signal is shaped to be of exponential form with an average decay constant of 11 μsec. The signal is fed to the main amplifier and is discriminated to give a square pulse after an amplification by a factor of 1000. The width of this pulse is proportional to the logarithm of the number of particles incident over the detector.

From January 24, 1995 onwards, the anode signals from 12 phototubes of each layer have been summed up and the shape of the sum pulse for each layer is recorded using a digital recorder with 20 nsec resolution. Before summing up signals from various detectors, the average amplitude of the signal due to a single muon from each detector has been adjusted to be same. The block diagram is shown in Fig. 4.

A. Density measurements

By controlling the high voltage for each photomultiplier, the peak value of the pulse width distribution is adjusted to be 10 μsec. The peak channel of the pulse width distribution nearly corresponds to the average energy loss of a muon passing vertically through the scintillator.

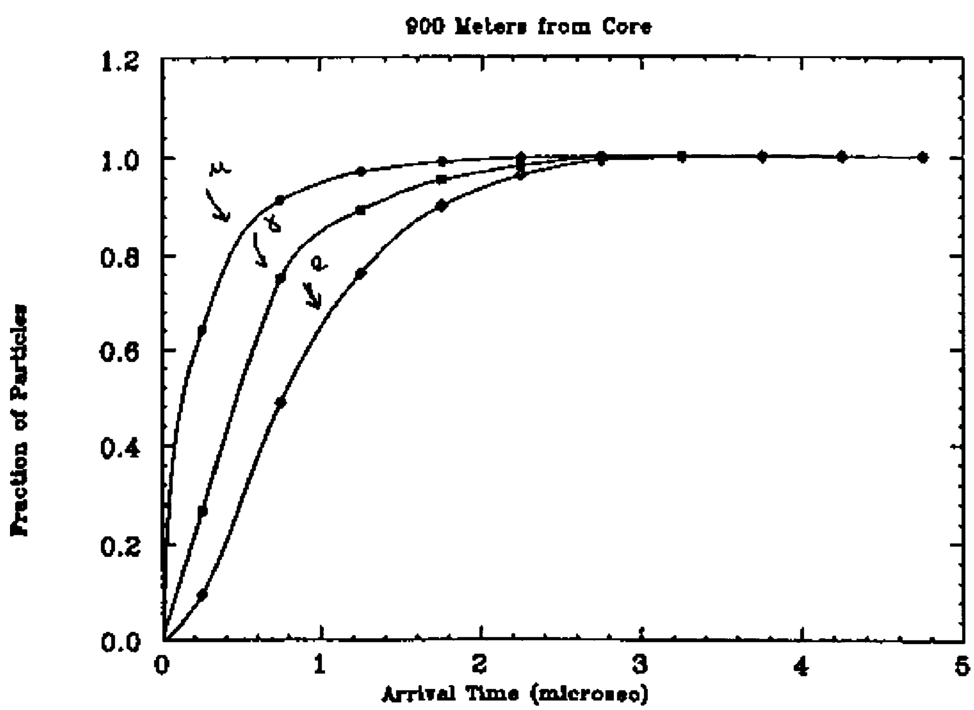

FIG. 2. Integral arrival time distributions for the three components. The diamonds, squares, and circles correspond respectively to photons, electrons/positrons, and muons. The muons arrive the earliest and at 900 m the arrival times of all the particles are spread over 2 μsec [8].

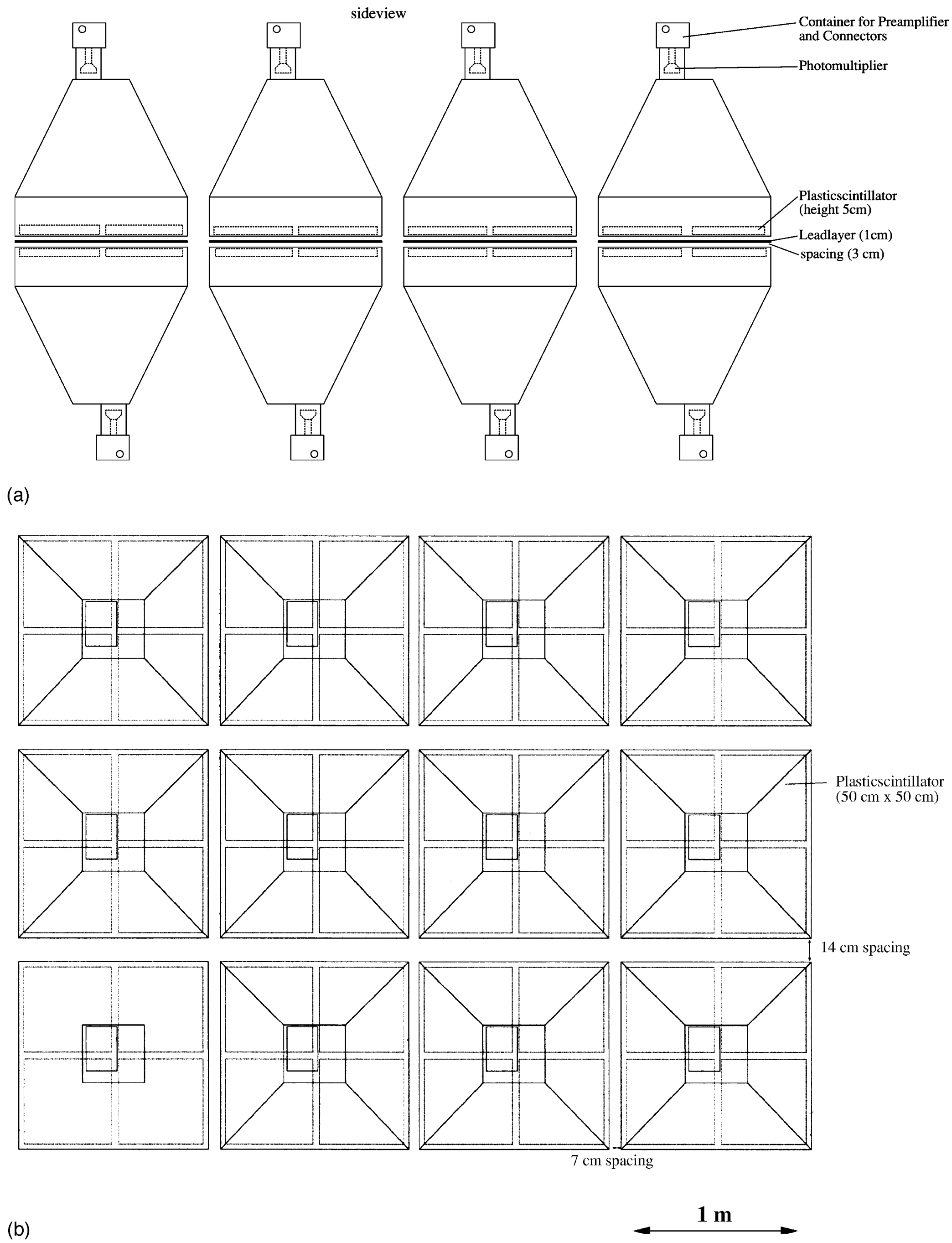

FIG. 3. Side and bird's-eye view of the sandwich detector.

B. Time response of the waveform recorder

The distributions of arrival times for the incident particles over the $12\,\mathrm{m}^2$ area of counters of the upper layer (top counters) and the lower layer (bottom counters) are recorded independently by a digital waveform recorder in each shower. The time profile of the signal is recorded during a time interval of 40 μsec before and after the trigger pulse. The observed distribution of the full width at half maximum (FWHM) values for waveforms recorded for top-bottom coincidence signals (coincident signals in both top and bottom counters, referred hereafter as a coincidence signal) is shown in Fig. 5. Distributions of integral pulse shape, defined as the summation of amplitudes (A_i) for n successive bins (in each 20 nsec) exceeding 3 mV ($\Sigma_{i=1}^{n(>3\,\mathrm{mV})}A_i$), are also shown. The peak value of the integral pulse shape distribution is used for the definition of a single particle.

These signals have been observed for events triggered by the AGASA; however, most of them are accidental ones. The median values for the distributions of peak value of signals, peak values of integral pulse shape distributions, and average values of FWHM and full width (FW) at 3 mV level of pulses are listed in Table I together with these of signal observed only by top counters (referred to hereafter as top-only signals) and bottom counters (referred to hereafter bottom-only signals). From the energy distributions of particles in Fig. 1, the most likely particles of coincidence, top-only, and bottom-only signals are muons, electrons, and photons, respectively.

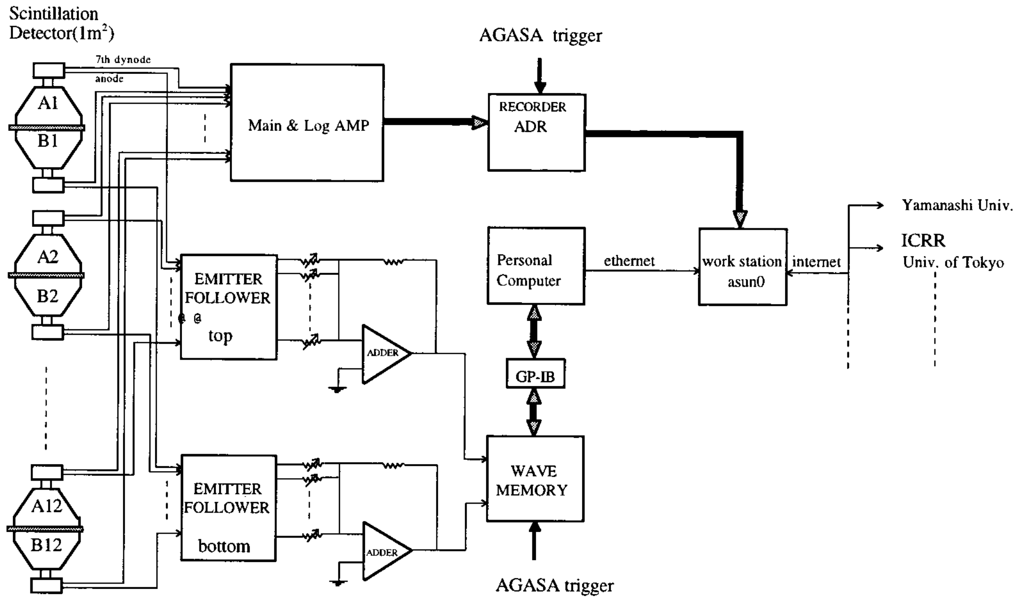

FIG. 4. Block diagram of the data acquisition system.

III. RESULTS

The experiment started September 24, 1994 and data collected until March, 1996 have been analyzed. Data from the waveform recorder are available from January 24, 1995 onwards. From all recorded data, only showers with energies larger than $10^{18.0}$ eV, zenith angles smaller than 45°, and cores hitting well inside the boundary of the Akeno branch of the AGASA have been used for the present analysis.

A. Examples of the observed events

Since most showers hit at core distances larger than 1000 m from the leadburger, the density values recorded are zero for most counters and only a few counters are hit by particles in each shower. If the observed density is smaller than 4 per 12 m^2, coincidence, top-only, and bottom-only signals can be easily distinguished from each other. In Fig. 6, an example of the leadburger data for a shower of $10^{18.2}$ eV is shown along with the energy losses in each of the top and bottom counters. One top-bottom coincidence signal, two top-only signals, and one bottom-only signal can be easily identified in this figure. The subtracted signal, obtained by subtracting the bottom layer signal from that of the top layer, is also displayed.

In Fig. 7, we show an example of a shower of $10^{19.4}$ eV, whose core distance from the leadburger is about 1500 m. The energy losses recorded in each counter are listed in the table of Fig. 7 and the arrival time distributions for both layers are shown over a range of 11 μsec. There are three clear signals which are delayed more than 3 μsec.

B. Energy deposit distribution for coincidence, top only, and bottom only signals

In order to see the energy loss distributions for muons, electrons, and photons far from the core, only showers with energy in the range, $10^{18.0}$–$10^{18.3}$ eV and core distances from the leadburger in the range 1000–2000 m are considered. Further, it is required that the number of hit counters be less than 4 out of 24 (20 before April 6, 1995). These distributions are displayed in Fig. 8, where the number of events in each energy loss bin (in units of 2 MeV) is plotted for the top-bottom coincidence, top-only, and bottom-only signals,

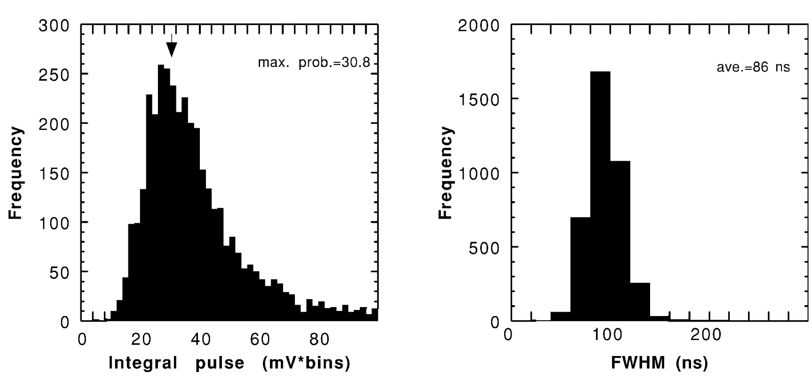

FIG. 5. Distributions of the integral pulse shape (left) and full width at half maximum, FWHM (right), for the top-bottom coincidence signals. The integral pulse shape is the amplitude (mV) summed over all time bins (in 20 nsec) exceeding 3 mV.

TABLE I. Median values for the distributions of peak value of signals, peak values of integral pulse shape distributions, and average values of the FWHM and full width (FW) at the 3 mV level of pulses for coincidence, top-only, and bottom-only signals. The values for the standard deviation for each distribution are also shown.

	Coincidence		Top only	Bottom only	Unit
	Top	Bottom			
Pulse amplitude	$8.8^{+3.0}_{-2.1}$	$8.6^{+4.0}_{-1.8}$	$9.4^{+4.6}_{-2.1}$	$9.8^{+5.4}_{-2.2}$	mV
Integral pulse shape	$30.8^{+20.4}_{-5.6}$	$28.1^{+21.5}_{-4.5}$	$32.1^{+26.6}_{-4.5}$	$30.0^{+31.5}_{-2.6}$	$\mathrm{mV}\times\left(\frac{\text{number of bins}}{20\ \text{nsec}}\right)$
FWHM	86^{+25}_{-6}	84^{+26}_{-8}	84^{+24}_{-5}	82^{+27}_{-7}	nsec
FW at 3 mV	116^{+30}_{-14}	110^{+27}_{-16}	117^{+33}_{-14}	112^{+31}_{-12}	nsec

respectively. The scintillators have a thickness of 5 cm corresponding to 5 g/cm^2 and thus an energy loss of 10 MeV for a charged particle passing in the perpendicular direction.

For the coincidence signals, the energy loss in the bottom counter has been plotted against the energy loss in the top counter on the top left of Fig. 8. Most of the points concentrated around an energy loss of 10 MeV in both counters are due to muons. However, some of the muons may be accompanied by electrons and/or photons in top or bottom counters and show a large discrepancy in energy losses between top and bottom counters.

The energy distributions of top-only and bottom-only signals are also displayed in the figure. The average values and standard deviations for these energy loss distributions for coincidence, top-only, and bottom-only signals are listed in Table II.

It is seen that the observed average energy loss of more than 12 MeV for these signals is larger than the expected values of 11 MeV after taking into consideration the zenith angle distribution of the observed showers. However, particles at a larger distance from the core are subject to larger scattering and they may be incident on the scintillator, on the average, at larger zenith angles than the zenith angle of the shower. The peaks of the energy distributions of the top-only and bottom-only signals are lower than that expected for muons. The spread of the bottom-only signals is significantly broader than others. This may be due to some of the photons getting converted into electrons by pair production or Compton scattering and traveling in the lead layer at large angles. These electrons would lose some energy in the lead or the iron cover of the bottom counter.

C. Accidental rates

In order to derive the lateral distribution and arrival time distribution of coincidence, top-only, and bottom-only signals, it is important to determine their accidental rates. These were determined from the rate of recording showers, with energies above $10^{17.5}$ eV, whose cores hit more than 3000 m from the detector, where the frequency of observed signals is almost independent of the core distance. The rates of accidental signals for the segmented density detectors per shower are listed in Table III. Total area of the leadburger was 10 m^2 from September 24, 1994 to April 6, 1995 and 12 m^2 afterwards: therefore, the average area is 11.3 m^2 for the present data set up to March, 1996.

This high accidental rate is due to the present gate width of 64 μsec for the density recorder for the leadburger counters, since the leadburger is located at a corner of the AGASA.

D. Arrival time distribution of the leadburger signals

Determination of arrival time distributions of top-bottom coincidence, top-only, and bottom-only signals is not straightforward. The distribution has been determined assuming that the earliest arriving particle in the top or bottom layer is not delayed. Therefore, if only one particle is observed, the particle is considered to have no delay for the arrival time distribution. In order to obtain the average arrival time distributions, leadburger densities per 12 m^2 observed within 3 μsec are used. The separation between coincidence, top-only, and bottom-only signals is made following the criteria which will be described later in Sec. IV A 2.

In Fig. 9, the average densities per m^2 are plotted for each 100 nsec time interval as a function of the arrival time, for showers with energies between $10^{18.0}$ and $10^{19.0}$ eV and core distance region $\log_{10}R=3.0-3.2$. Accidental rates per m$^2\times$100 nsec are listed in Table IV and these are extracted in the figure. The average energy of primary particles is about $10^{18.3}$ eV and the solid lines are the expected values from simulation normalized to $10^{18.3}$ eV at $\log_{10} R=3.1$. The large difference from solid lines within 500 nsec is due to the experimental limitation of the defining the earliest arriving particle described above. The implications of the results will be discussed in Sec. IV B.

IV. DISCUSSION

A. Lateral distributions of coincidence, top-only, and bottom-only signals

1. From segmented density detectors

In Fig. 10, the densities of top-bottom coincidence, top-only, and bottom-only signals are plotted by closed circles as a function of core distance. The density values have been derived using the same set of showers as used for obtaining Fig. 8, but showers have been grouped into four core distance bins. The following criteria have been taken into consideration.

(1) Every signal is assumed to be due to a single particle, irrespective of its energy loss.

(2) Background counts, listed in Table III, are subtracted.

(3) Arrival time information is not used.

For these plots, only showers with energies between $10^{18.0}$ and $10^{18.3}$ eV have been used and the average energy of the

segment No.	1	2	3	4	5	6	7	8	9	10	11	12
top	1.5	0.0	0.0	0.0	0.0	0.0	1.1	0.0	0.0	0.0	0.98	0.0
bottom	0.0	0.0	0.0	0.0	0.0	0.0	0.0	0.0	0.0	0.70	0.91	0. 0

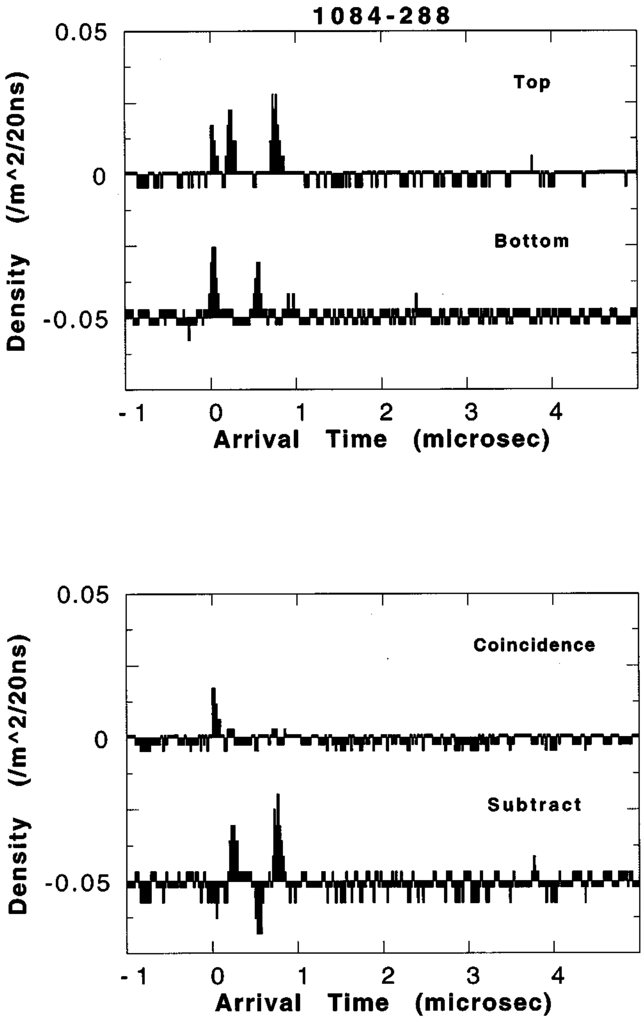

FIG. 6. An example of data from the leadburger for a shower with core at 1240 m and energy of $10^{18.2}$ eV incident at 17.8° zenith angle. The upper figure shows the arrival time distribution for top and bottom counters with 20 nsec resolution over 6 μsec. The upper distribution in the lower figure is the coincident part between the top and bottom layers while the lower one represents the difference obtained by subtracting the signal in the bottom layer from the top layer.

segment No.	1	2	3	4	5	6	7	8	9	10	11	12
top	2.3	1.7	1.5	7.5	0.69	14.1	4.6	3.0	4.1	1.0	2.6	0.76
bottom	1.2	2.1	1.4	1.2	1.3	1.4	1.4	0.0	4.6	1.1	1.2	0.0

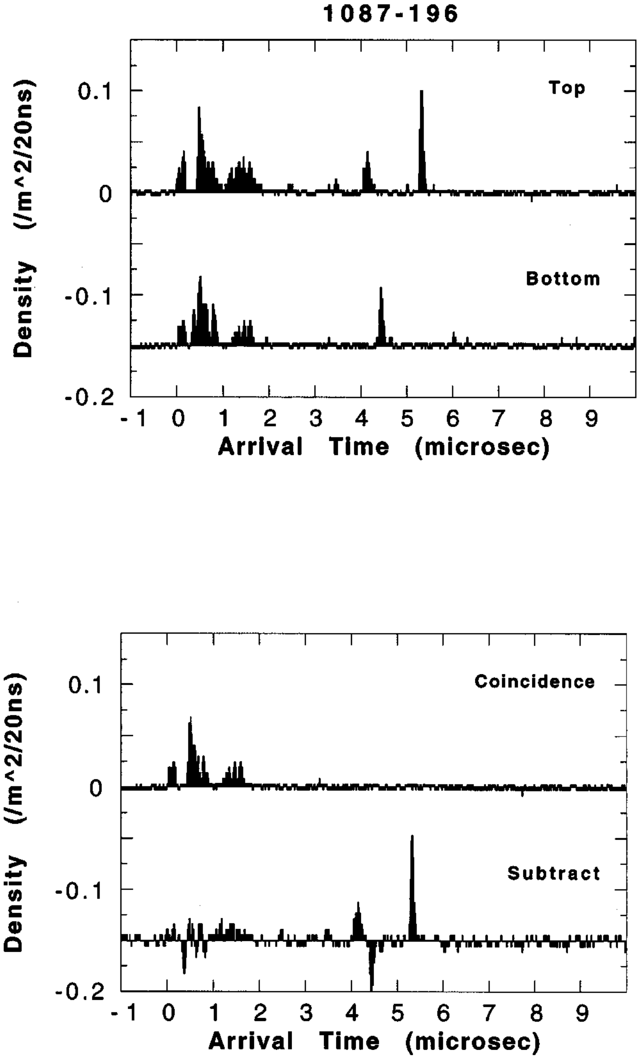

FIG. 7. An example of a large event, $E=10^{19.4}$ eV, zenith angle$=34.7°$, and $R=1509$ m.

primary particles is $10^{18.13}$ eV and is normalized to $10^{18.2}$ eV. If we derive densities by dividing the average energy loss in the observed distribution by the average energy loss for a single particle derived in Table II, the coincidence density increases by a factor of 1.1, while top-only and bottom-only densities do not change. However, since some of the top-only or bottom-only signals may be included in the coincidence signals, the plotted frequency may be the lower limit of the real one.

2. From waveform recorder data

In order to interpret the waveform data, the amplitude of the arrival time distribution of the bottom layer is subtracted from that of the top layer, as displayed in Figs. 6 and 7. If there are no fluctuations in the energy loss in the top and bottom layers, a coincidence signal must show no surplus in the subtracted result. A positive signal in the subtracted distribution may be interpreted as a top-only signal and a negative signal as a bottom-only signal. Since there are fluctuations, not only in the energy loss but also in the FWHM for a single particle, we adopt the following guidelines.

(1) If a top signal does not coincide with a bottom signal and its integral pulse shape $\geqslant 0.3$ particles ($\Sigma_{i=1}^{n>3\,\mathrm{mV}} A_i$) and its FWHM $\geqslant 60$ nsec, then we regard it as a top-only or a bottom-only signal.

(2) If the FWHM of a top-bottom coincidence signal (common part of top and bottom signals) is greater than 60 nsec, we regard it as a coincidence signal.

(3) The numbers of particles of coincidence, top-only, and bottom-only are estimated from the average values of the integral pulse shape listed in Table I.

(4) The accidental coincidences are subtracted.

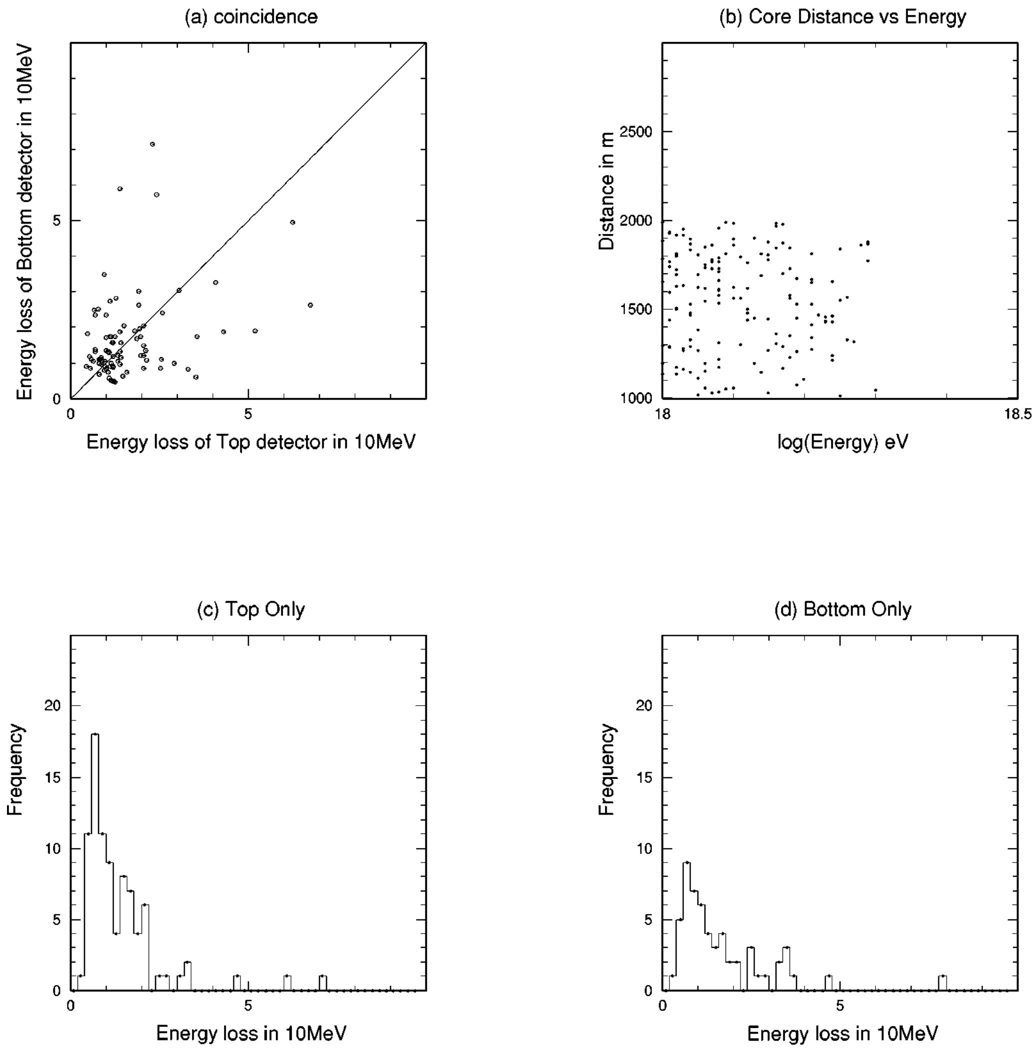

FIG. 8. (a) Correlation of energy losses of bottom detector and top detector. Distribution of energy loss for top-only signals (c) and bottom-only signals (d). Relation between energy and core distance of leadburger of selected showers is shown in (b).

Lateral distributions of coincidence, top-only, and bottom-only signals determined from the waveform recorder data, following the above guidelines, are plotted as open circles, open squares, and crosses, respectively, in Fig. 10. For this analysis we have used all showers between $10^{18.0}$ and $10^{19.0}$ eV. The average energy is about $10^{18.3}$ eV and is normalized to $10^{18.2}$ eV.

3. Comparison of muons above 0.5 GeV

It is seen that densities determined by the segmented density detectors without timing information and by a nonsegmented waveform recorder coincide rather well with each other as far as densities are low. In Fig. 10(a), a solid line is a lateral distribution of muons above 0.5 GeV determined by AGASA muon detectors [12]. The present result is a little higher (about 25–40%) than that above 0.5 GeV. The difference can be explained by electrons of energies of more than 40 MeV, since the contribution of muons less than 0.5 GeV may be negligible. That is, muons can be well separated from electromagnetic components with contamination of 25–40% electromagnetic components with 1 cm lead at farther than 1 km from the core.

TABLE II. The average values and standard deviations for the energy loss distributions for coincidence, top-only, and bottom-only signals in units of 10 MeV.

		Peak	Average	σ
Coincidence	Top counter	1.0	1.32	0.71
	Bottom counter	1.0	1.41	0.75
Top only		0.75	1.25	0.82
Bottom only		0.80	1.56	1.05

4. Expected lateral distribution from MOCCA simulation

The expected densities of coincidence, top-only, and bottom-only signals are estimated from the results from proton and iron primaries provided by Cronin [13] which were

TABLE III. The rates of accidental signals per shower.

Coincidence	0.125 ± 0.020
Top only	0.090 ± 0.019
Bottom only	0.105 ± 0.020

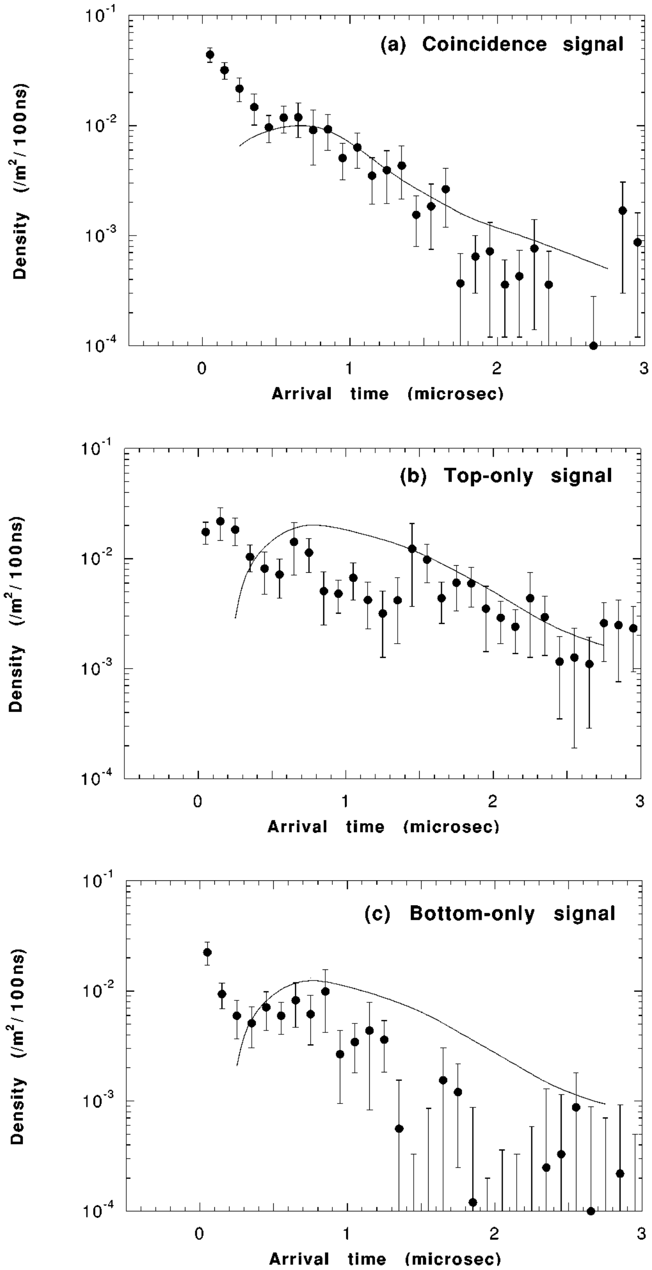

FIG. 9. Arrival time distributions for the coincidence (a), top-only (b), and bottom-only (c) signals. The first recorded particle in each shower is considered not to be delayed. The core distance range is between 1000 m and 1584 m. Lines represent the expectations from simulations at 1260 m provided by Cronin [13] for showers initiated by 10^{19} eV protons. The average energy for the experimental data is $10^{18.3}$ eV and simulation results are normalized to $10^{18.3}$ eV.

simulated using the MOCCA program. The results for incident showers of primary proton and iron nucleus with energy 10^{19} eV at a zenith angle of 0° are used.

Each density is evaluated as follows.

(1) Top-bottom coincidence signals: Muons and electrons of energies larger than 40 MeV at each distance bin are summed.

(2) Top-only signals: Electrons with energies between 2.5 and 40 MeV, which corresponds to the energy passing through the top scintillator box wall, but stopping before the bottom scintillator, and electrons converted from photons of energies between 5 MeV and 40 MeV in a 5 cm scintillator are summed at each distance bin.

(3) Bottom-only signals: By dividing 1 cm lead shield into five layers, the number of electrons, which are produced by Compton scattering or pair production of photons in each layer and traverse through the rest of the lead layer, has been estimated[1] and the numbers of electrons from all layers have been summed at each distance bin. All electrons converted from photons above the lead layer are neglected.

TABLE IV. Rates of accidental signals per $m^2 \times 100$ nsec.

Coincidence	5.5×10^{-4}
Top only	5.4×10^{-3}
Bottom only	5.3×10^{-3}

To normalize the simulation results of 10^{19} eV to those of $10^{18.2}$ eV, electromagnetic components are reduced linearly with energy: however, muons are reduced by assuming a relation $\rho_\mu \sim E^{0.82}$, irrespective of core distance, from the experimental relation $N_\mu \sim E^{0.82}$ obtained at Akeno [12]. The simulation results are compared with the experiment in Figs. 10(b), 10(c), and 10(d).

The expected coincidence signals from primary protons are about 50–60% lower than those from primary iron nuclei, while those of bottom-only and top-only signals from protons are similar to those from iron nuclei within 10%. This is the reason why the density of electromagnetic components far from the core is a good parameter of energy estimation irrespective of primary composition. The observed coincidence signals are in good agreement with the simulation from protons, while top-only and bottom-only signals are a factor of 1.5–2.0 lower than that from simulations. Some part of these discrepancies may be due to the difficulty of selecting top-only and bottom-only signals from coincident signals by the present subtraction method of upper-layer signals from lower-layer signals. This can be understood from the energy loss distributions of top and bottom counters for coincidence signals in Fig. 8(a), where about 20–30% of coincident events are found to be accompanied by electrons and/or photons in top and/or bottom counters.

Though the observed coincident signals agree well with expected signals from the proton primary composition, we need further study in both experiment and simulation, considering uncertainties assumed for the derivation of both experimental and simulation results, to confirm the primary composition.

B. Arrival time distributions of top-only, bottom-only, and coincidence signals

In Fig. 9, the average observed densities per m^2 per 100 nsec are compared with the results obtained from simulations for proton primaries [13]. The lines in these figures represent

[1]The scattering angle of an electron is neglected. If the scattering angle is taken into account, the minimum energy of the produced electron passing through the shield increases and hence the densities of expected bottom-only signals may be decreased.

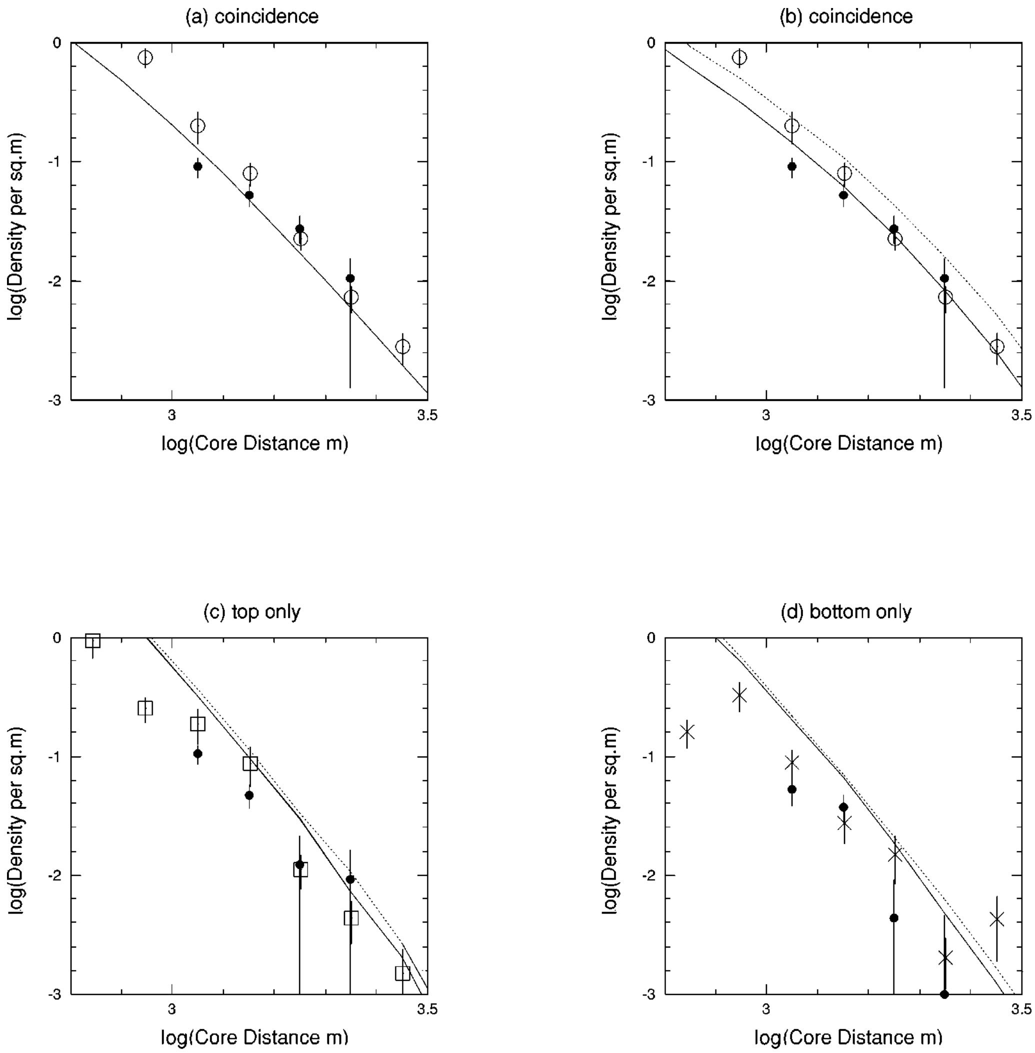

FIG. 10. Lateral distributions for the top-only [open squares in (c)] and bottom-only signals [crosses in (d)] as well as the coincidence events [open circles in (a) and (b)], determined from waveform records of top and bottom layers. Solid circles are those determined from segmented density detectors. The solid line in (a) represents the experimental results of muons above 0.5 GeV by AGASA muon detectors. Solid lines in other figures and dotted lines represent the expected distributions for the coincidence (b), top-only (c), and bottom-only (d), respectively, estimated from simulation results of proton primary and iron primary compositions, respectively, provided by Cronin [13] (all normalized to $10^{18.2}$ eV).

the results from simulations at a core distance of 1260 m. The primary energy for simulation results is normalized to $10^{18.3}$ eV and the expected density is adjusted to that in 100 nsec. Since the delay time is considered to be zero for the incidence of a single particle in the experiment, the experimental and simulation results cannot be compared directly with each other, especially in the time region of 0–500 nsec, while above 500 nsec, the observed arrival time distribution

TABLE V. Details of particles delayed by more than 3 μsec.

Event number	Primary Energy E (eV)	Top/bottom	Distance (m)	Energy loss (10 MeV)	Delay (μsec)	FWHM (nsec)
No. 27582-2847	25.0	top only	1509	2.9	4.04	140
LB1087-196		top only		5.4	5.26	80
		bottom only		3.1	4.38	80
		Yamanashi	1630	1.3	3.1	100
		30 m^2		1.2	4.0	100
		detector		1.5	7.8	100
		(50 nsec time		1.8	8.2	100
		resolution		11.1	10.0	100

TABLE VI. Number of delayed particles observed in different delay time and energy loss bins, measured by the Yamanashi arrival-time detector of 30 m^2 area over 7.7 years.

$E \geqslant 10^{19}$ eV, $R \geqslant 1000$ m, $\theta \leqslant 45°$					
	Energy loss in units of 10 MeV				
Delay time (μsec)	1–2	2–3	3–5	5–10	⩾10
3.0–4.0	6	1	2	0	3
4.0–5.0	1	2	1	1	0
5.0–6.0	1	3	1	1	0
6.0–7.0	0	1	0	0	0
7.0–8.0	1	0	0	1	0
8.0–9.0	1	0	0	0	0
9.0–10.0	0	0	0	0	0

of coincident signals, which are mainly muons, is well reproduced by simulation. The shapes of the arrival time distribution of top-only (mainly electrons) and bottom-only (mainly photons) signals are consistent with the simulated ones within experimental errors, though there are discrepancies in absolute values between experiment and simulation due to the similar reason discussed in the previous section.

C. Delayed particles

In Table V, particles delayed by more than 3 μsec are listed for the event of $10^{19.4}$ eV at 1509 m from the core, whose data are shown in Fig. 7. For reference, delayed signals of this event recorded by the Yamanashi arrival-time detector of 30 m^2 area, operated since June, 1986 [14], are also listed in Table V.

According to the analysis of the Yamanashi detector data from June, 1986 to March, 1994, the number of showers associated with particles with delay of more than 3 μsec and with more than 10 MeV energy loss is 12 among a total of 17 showers of energies larger than 10^{19} eV and with core distances farther than 1000 m and zenith angles smaller than 45°.

The relation between delay time and energy loss, in units of 10 MeV, is listed in Table VI. Particles with a delay larger than 9 μsec were not found so far and have been seen only in this event (No. 27582-2847) observed recently.

The median and the average energy losses for these delayed particles are about 25 and 40 MeV, respectively. This amount of energy loss is expected for recoiling protons generated by neutrons in the scintillator of 5 cm thickness and hence they are most likely due to neutrons. If these delayed signals are indeed due to neutrons, they may not be observed in a water Čerenkov detector which is proposed to be used in the Auger Project and its prototype is in operation at Akeno [15].

V. CONCLUSIONS

Data collected over the 18-month run of a detector with two scintillators sandwiching a 1.8 radiation length lead plate triggered by the AGASA have been analyzed and show interesting information on electrons, photons, and muons at around 1000–2500 m from the core for showers of energies larger than $10^{18.0}$ eV. The lateral distribution and arrival time distribution of coincidence signals represent that of muons with a contamination of 25–40% electromagnetic components. The results agree well with the expected signals from proton primary from simulation using the MOCCA program: however, we need further study in both experiment and simulation, considering uncertainties assumed for the derivation of both experimental and simulation results. Both top-only and bottom-only signals are a factor of 1.5–2.0 lower than that from simulations. Some part of these discrepancies may be due to the difficulty of separating electromagnetic components from coincidence signals.

Considering that the performance of the sandwich detector is reproduced rather well by the simulations, the MOCCA program may be used as a powerful tool for the design work for a water Cerenkov detector, which is proposed to be used in the Auger Project.

It is important to measure the fluctuations in the ratio of the muonic and electromagnetic components on a shower-to-shower basis in order to know how effective a ratio of the muon/electromagnetic components is in estimating the average mass composition of highest energy primary cosmic rays. Recently the Osaka City University group has constructed another leadburger of 12.5 m^2 area segmented into fifty 0.25 m^2 at about 1.7 km from the present one. This detector may be much powerful to separate muons from electromagnetic components and to measure the fluctuations on shower to shower for 10^{19} eV and we are continuing the experiment in collaboration with them.

ACKNOWLEDGMENTS

We wish to thank Professors J. W. Cronin and A. A. Watson for encouraging us to perform this experiment and Professor J. W. Cronin for providing us compiled data sets of simulation results. We are also grateful to all AGASA members for providing us AGASA data, especially to M. Teshima for air shower analysis and R. Torii for preparation of 1 km^2 data. We would like to thank Professor S. Tonwar for his kind improvements and valuable advice on the manuscript.

[1] K. Greisen, Phys. Rev. Lett. **16**, 748 (1966).
[2] G. T. Zatsepin and V. A. Kuźmin, Pis'ma Zh. Eksp. Teor. Fiz. 4, 114 (1966) [JETP Lett. **4**, 78 (1997)].
[3] M. Teshima, in *Proceedings of the 23rd ICRC, Invited, Rapporteur, and Highlight papers, 1993*, edited by D. A. Leahy, R. B. Hicks, and D. Venkatesan (World Scientific, Singapore, 1994), p. 257.
[4] D. J. Bird *et al.*, Astrophys. J. **424**, 491 (1994).
[5] N. Hayashida *et al.*, Phys. Rev. Lett. **73**, 3491 (1994).
[6] N. Hayashida *et al.*, Phys. Rev. Lett. **77**, 1000 (1996).
[7] J. W. Cronin, University of Chicago Report No. EFI92-8, 1992.
[8] J. W. Cronin, contribution to Snowmass Report on Cosmic Rays, report, 1994.

[9] A. M. Hillas, in Proceedings of the 12th ICRC, Hobart, 1971, Vol. 3, p. 1001.
[10] Design Report of the Pierre Auger Project, 1995.
[11] N. Chiba *et al.*, Nucl. Instrum. Methods Phys. Res. A **311**, 338 (1992).
[12] N. Hayashida *et al.*, J. Phys. G **21**, 1101 (1995).
[13] J. W. Cronin (private communication).
[14] K. Honda *et al.*, in Proeedings of the 23rd ICRC, Calgary, 1993, Vol. 4, p. 311.
[15] N. Sakaki and M. Nagano, in *Proeedings of the International Symposium on Extremely High Energy Cosmic Ray: Astrophysics and Future Observatories*, edited by M. Nagano (Institute of Cosmic Ray Research, University of Tokyo, Tokyo, 1997), p. 402.